A Federated Learning Framework for Disease Diagnosis under Non-IID Data

Wenhui Sun[1] and Xuebin Ma[1]

[1] Wireless Networking and Mobile Computing Laboratory Inner Mongolia University, Hohhot 010000, China
swhemail1@163.com
csmaxuebin@imu.edu.cn

Abstract. Federated learning has become one of the common frameworks for disease diagnosis because of its characteristics of protecting the privacy of local data and overcoming data islands. Recently, many disease diagnosis methods based on federated learning have been proposed, but most of them do not aim at the characteristics of non-independent and identically distributed (non-IID). Therefore, this paper proposes a disease diagnosis framework based on federated learning to improve the accuracy of disease prediction under non-IID. This framework has two main innovations: data sharing strategy method and image segmentation model. In the data distribution, it can improve the prediction accuracy when the data are not independent and identically distributed. In the stage of image segmentation, this paper proposes D-Net, which can realize the accurate segmentation of the image under the condition of low parameters. Finally, the experimental results on the datasets show that this framework can improve the accuracy of disease diagnosis.

Keywords: Federated Learning, Image Segmentation Network, Data Sharing Strategy, Disease Diagnosis.

1 INTRODUCTION

Currently data islands and privacy leaks are very serious in the medical field[1-2]. Federated learning is proposed in order to protect users' privacy and break the barrier of data island. Federated learning is a distributed machine learning framework which can not only use data for model training, but also meet the requirements of multiple institutions to protect user privacy, information security, and government privacy protection. However, federated learning faces severe challenges brought by the problem of data non independent and identically distributed. Data non independent and identically distributed refers to the great difference in the distribution of data. Medical data are in line with the above characteristics.

Therefore, we propose a disease diagnosis framework based on federated learning. The main contributions of this paper are summarized as follows:

(1) Data sharing strategy can improve the prediction accuracy in the case of data islands and non-IID data.

(2) Image segmentation model. It alleviates the unknown network depth through effective integration, redesigns the hop to aggregate features with different semantic scales on the decoder sub network, so as to produce a highly flexible feature fusion scheme on the basis of enhancing the organ boundary.

The rest of this paper is organized as follows. Section 2 introduces related work on non-IID and image segmentation under the federal learning framework. Section 3 presents some related basics a of non-IID and image segmentation. Section 4 details the data distribution strategy. Section 5 describes the detailed the structure of the image segmentation model. Section 6 analyzes and summarizes the experimental results; finally, section 7 is the conclusion of this paper.

2 RELATED WORK

Facing the problem of non-IID data under the federal learning framework and medical image segmentation, many methods have been proposed.

2.1 Data non independent and identically distributed

McMahan et al. [3] introduced the concept of FL based on data parallelism and proposed a Federated Averaging algorithm to approach the non-IID challenge. FedAvg allows multiple devices to train a machine learning model cooperatively, while keeping the user data stored locally, obviates the need for uploading the users' sensitive data to a centralized server, and makes it possible for the edge devices to train a shared model locally within their own local dataset. FedAvg meets the basic requirements for privacy protection and data security by aggregating the updates (gradients) of local models. However, the accuracy of convolutional neural networks trained with FedAvg can reduce significantly.

Smith et al. [4] proposed a multi-task learning (MTL) framework and developed MOCHA to address system challenges in MTL. Due to the use of primal–dual optimization method, MOCHA generates separated but related models for each client, which makes it unsuitable for non-convex optimization tasks.

Federated learning relies on stochastic gradient descent (SGD), which is widely used in training deep networks with good empirical performances [5]. The IID sampling of the training data is important to ensure that the stochastic gradient is an unbiased estimate of the full gradient. In practice, it is unrealistic to assume that the local data on each edge device is always IID.

Zhao et al. [6] proposed accuracy reduction can be explained by the weight divergence, which can be quantified by the earth mover's distance (EMD) between the distribution over classes on each device and the population distribution. Experiments show that accuracy can be increased for the CIFAR-10 dataset.

Naoya Yoshida et al. [7] proposed a hybrid learning mechanism referred to as Hybrid-FL, wherein the server updates the model using the data gathered from the clients and aggregates the model with the models trained by clients. Hybrid-FL solves both client- and data-selection problems via heuristic algorithms. The algorithms

increase the number of clients participating in FL and make more data gathered in the server IID, thereby improving the prediction accuracy of the aggregated model.

Tiffany Tuor et al. [8] proposed a method for selecting relevant data, which use a benchmark model trained on a small benchmark dataset that is task-specific, to evaluate the relevance of individual data samples at each client and select the data with sufficiently high relevance.

To sum up, the research is based on the establishment of shared dataset, considering how to establish a shared dataset, and did not consider strategy to distribute the shared dataset, so this we propose the data sharing strategy.

2.2 Image segmentation

Image segmentation model includes traditional segmentation model and deep learning model. Traditional image segmentation methods are introduced according to 6 types of methods based on thresholds, edges, regions, clusters, graph theory, and specific theories.

In deep learning model, Olaf Ronneberger et al. [9] proposed U-net network structure, which integrates the characteristics of different network levels and improves the calculation accuracy; the flexible network structure combined with in-depth supervision can greatly reduce the amount of parameters of in-depth network within an acceptable range, but its disadvantage is that the network depth is not enough, resulting in general performance in multi classification .

Ozan Oktay et al. [10] proposed Attention U-Net network structure. U-Net with soft attention is used to supervise the characteristics of the upper level through the characteristics of the lower level to realize the attention mechanism (limit the activated part to the area with segmentation, reduce the activation value of the background to optimize the segmentation and realize end-to-end segmentation).

Zahangir Alom et al. [11] proposed R2U-Net network structure for medical image segmentation, replacing the basic convolution unit in U-Net with cyclic residual convolution unit, so as to enhance the integration ability of context information. In addition, R2U-Net network adopts attention gates (AGS) instead of the original skip connection, and the segmentation effect is better than that of U-Net. Its disadvantage is that the size and parameters of the model are much larger than those of U-Net.

Gu Z et al. [12] proposed a context encoder network (referred to as CE-Net) to capture more high-level information and preserve spatial information for 2D medical image segmentation. CE-Net mainly contains three major components: a feature encoder module, a context extractor and a feature decoder module. CE-Net uses pretrained ResNet block as the fixed feature extractor. The context extractor module is formed by a newly proposed dense atrous convolution (DAC) block and residual multi-kernel pooling (RMP) block.

Zhou et al. [13] proposed the UNet++ network structure to alleviate the unknown network depth through the effective integration of U-Nets with different depths. These U-Nets can partially share an encoder, and can conduct joint learning through depth supervision at the same time, redesign skip connections to aggregate features of varying semantic scales at the decoder subnetworks, so as to produce a highly flexible feature fusion scheme. A pruning scheme is proposed to speed up the reasoning speed of

UNet++. However, it does not explore sufficient information from full scales and there is still a large room for improvement.

Huang et al. [14] proposed a novel UNet 3+, which takes advantage of full-scale skip connections and deep supervisions. The full-scale skip connections incorporate low-level details with high-level semantics from feature maps in different scales; while the deep supervision learns hierarchical representations from the full-scale aggregated feature maps. They propose a hybrid loss function and devise a classification-guided module to enhance the organ boundary and reduce the over-segmentation in a non-organ image, yielding more accurate segmentation results. Its disadvantage is that the number of network layers is not deepened, so it cannot adapt to multiple types of datasets. However, its network layers are not deepened, so it cannot adapt to multiple types of datasets.

Qin X et al. [15] proposed U^2-Net which is a two-level nested U-structure. It is able to capture more contextual information from different scales thanks to the mixture of receptive fields of different sizes in residual U-blocks (RSU). However, its model size is much larger than that of U-Net.

Above all, the above research lacked a highly integrated, flexible and efficient semantic feature fusion scheme based on enhancing the organ boundary, so we propose a image segmentation model called D-Net.

3 Preliminaries

Definition 1. Data non-IID. Federated learning aims to train a global model, which can train the data distributed on different devices while protecting data privacy [16]. At the same time, federated learning faces statistical challenges. Each client data of federated learning depends heavily on the characteristics of specific local devices. Therefore, the data distribution of connected clients may be completely different. This phenomenon is called non-independent and identically distributed (non-IID). It can lead to serious model divergence.

Definition 2. Image segmentation refers to segmentation at the pixel level according to the features presented by the image (such as image texture, gray scale), in which the segmented regions do not coincide with each other. The image features in the same region are similar and have different features in different regions.

4 METHOD

4.1 Data Sharing Strategy

The basic framework of shared data distribution strategy is federal learning framework. Based on the federal learning framework, the data distribution strategy is carried out. The detailed steps are as follows:

(1) Build a shared dataset.
(2) Initialize the model.
(3) The server chooses the client at random. For example, there are a total of 100 clients, and 10% of the clients are randomly selected as the clients for this training, that is, 10 clients are used as the clients for this training.

(4) If the epoch is 1, the server sends the model to the selected client (in the following steps, the client is the selected client).
(5) The client downloads the model and uses the local data for training until the model converges, calculates the accuracy after the training, and uploads the model and accuracy after the client has finished training to the server.
(6) The server calculates the average accuracy rate according to the accuracy uploaded by each client, and updates the global model.
(7) Before running the second epoch, the server calculates the data volume of the shared dataset sent to the client according to the average accuracy. If the accuracy of a client is less than the average accuracy, then send m pieces of data to the client. Its formula is as follows: $m = i \times n$, where the $i = \frac{acc_{avg} - acc_i}{acc_{avg} - acc_{min}}$, n indicates the shared dataset size. If the accuracy of a client is greater than or equal to the average accuracy, the shared dataset will not be delivered.
(8) Client accepts shared data.
(9) The client will share data and local data to train together until convergence.
(10) The client uploads the client model to the server.
(11) The server determines whether the epoch is greater than n (n is the preset number of server training), if it is greater than n, the training ends; if it is less than n, go to step 9.

4.2 Image Segmentation Model

Before judging the disease, the medical image needs to be segmented. A new segmentation model called D-Unet is proposed in this paper. The model adopts the encoder decoder topology and their structure is shown in Fig. 1. Main features of this model are as follows:

(1) Based on UNet 3+, the two depth models are effectively integrated to alleviate the unknown network depth.
(2) The two depth models share the encoder, realize sharing the encoder, and learn at the same time through depth supervision.
(3) Redesign the jump connection and aggregate the semantic features on different scales to produce a flexible fusion scheme.

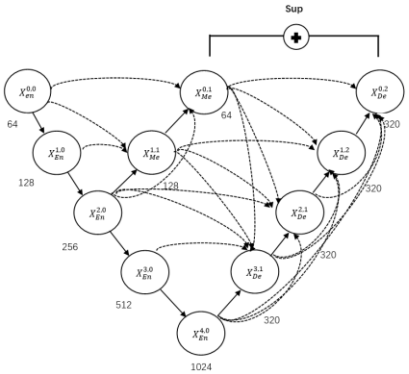

Fig. 1. Model diagram

A. Model Structure

Take $X_{Me}^{1,1}$ as an example to explain the structure of three-layer D-Unet. Similar to the UNet, the feature map from the same-scale encoder layer $X_{En}^{1,0}$ are directly received in the decoder. In contrast to the UNet, a set of inter encoder-decode skip connections delivers the low-level detailed information from the smaller-scale encoder layer $X_{En}^{0,0}$ by applying non-overlapping max pooling operation; while a chain of intra decoder skip connections transmits the high-level semantic information from larger-scale decoder layer $X_{En}^{2,0}$, by utilizing bilinear interpolation. With the three same-resolution feature maps in hand, we need to further unify the number of channels, as well as reduce the superfluous information. According to the experience of UNet 3+, this segmentation model also uses a 3 × 3 filter for convolution operation.

Take $X_{Dn}^{2,1}$ as an example to explain the structure of five-layer D-Unet. Similar to the UNet, the feature map from the same-scale encoder layer $X_{En}^{2,0}$ are directly received in the decoder. In contrast to the UNet, a set of inter encoder-decode skip connections delivers the low-level detailed information from the smaller-scale encoder layer $X_{Me}^{0,1}$ and $X_{Me}^{1,1}$, by applying non-overlapping max pooling operation; while a chain of intra decoder skip connections transmits the high-level semantic information from larger-scale decoder layer $X_{En}^{4,0}$ and $X_{De}^{3,1}$, by utilizing bilinear interpolation. With the five same-resolution feature maps in hand, we need to further unify the number of channels, as well as reduce the superfluous information. In order to unify the number of channels and reduce redundant information, 64 filter of size 3 × 3 for convolution. To seamlessly merge the shallow exquisite information with deep semantic information, we further perform a feature aggregation mechanism on the concatenated feature map from five scales, which consists of 320 filters of size 3 × 3, a batch normalization and a ReLU activation function.

B. Deep Supervision

We adopt the way of double supervision. The first priority is to adopt full-scale deep supervision similar to that in UNet 3+, which the last layer of each decoder stage is fed into a plain 3 × 3 convolution layer followed by a bilinear up-sampling and a sigmoid function. The second supervision adopts a supervision method similar to UNet++, using a 1×1 convolution with C kernels follwed by a sigmoid activation function to aggregate the information of $X_{Me}^{0,1}$ and $X_{Me}^{0,2}$.

The loss function is a hybrid segmentation loss function, which is composed of pixel cross entropy loss function and dice loss function. The hybrid loss may take advantages of what both loss functions have to offer: smooth gradient and handling of class imbalance. Mathematically, the hybrid loss is defined as:

$$L(Y,P) = -\frac{1}{n}\sum_{c=1}^{C}\sum_{n=1}^{N}\left(y_{n,c}\log P_{n,c} + \frac{2y_{n,c}P_{n,c}}{y_{n,c}^2 + P_{n,c}^2}\right) \quad (1)$$

where $y_{n,c} \in$ Y and $P_{n,c} \in$P denote the target labels and predicted probabilities for class c and n^{th} pixel in the batch, N indicates the number of pixels within one batch. The overall loss function for D-Unet is then defined as the weighted summation of the hybrid loss from each individual decoder:

$$L = \sum_{i=0}^{d} \eta_i \cdot L(Y, P_i) \tag{2}$$

where d indexes the decoder. In the experiments, we give same balanced weights η_i to each loss, i.e., $\eta_i \equiv 1$, and do not process the ground truth for different outputs supervision like Gaussian blur.

5 EXPERIMENTAL RESULTS

5.1 Data Distribution Strategy

A. Datasets

In this section, experiments are carried out on two datasets. They are 2D COVID-19 dataset [17] and MNIST dataset [18].

B. Evaluation Metrics

For quantitative analysis of the experimental results, several performance metrics are considered, including Accuracy and Loss. To do this we also use the variables True Positive (TP), True Negative (TN), False Positive (FP), and False Negative (FN). The overall accuracy is calculated using Eq. (3).

$$\text{Accuracy} = \frac{TP + TN}{TP + TN + FP + FN} \tag{3}$$

The loss is calculated using Eq. (4). Where c represents the number of categories; $\hat{y}$ Indicates the real category. If it belongs to the current category i, it is 1; otherwise, it is 0; y represents the probability that the prediction output belongs to category i. If there are 10 categories, there must be y according to the constraint with a total probability of y_0+y_1+···+y_9=1.

$$Loss = -\sum_{i=0}^{c} \hat{y} \log y_i \tag{4}$$

C. Experimental analysis

Under the framework of federal learning, we experiment with different non-IID forms. The parameters of this experiment are the optimization function, SGD function and cross entropy loss function.

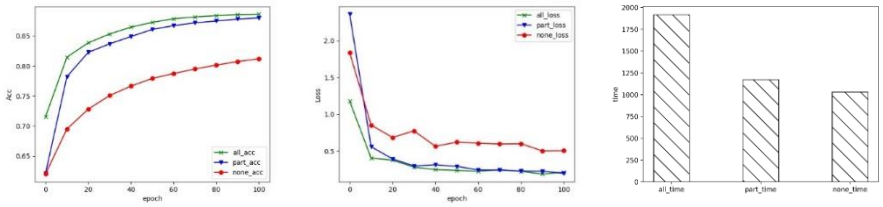

(a) Accuracy (b)Loss (c)Running time

Fig. 2. Results of 2D COVID-19 pneumonia dataset are shown in the same number and distribution

In the case of the same number and distribution, the results of 2D COVID-19 dataset are shown in Fig. 2. In this experiment, the accuracy and loss value are evaluated respectively. In terms of prediction accuracy, the accuracy of part-distributed is similar to that of all-distributed. There is a big gap between non-distributed and the other two cases, with a difference of 7%. the downward trend of all-distributed and part-distributed loss functions basically coincides and is basically stable, and the values are roughly the same in terms of loss value. The overall difference between the loss value of the non-distributed and the other two cases is about 0.2.

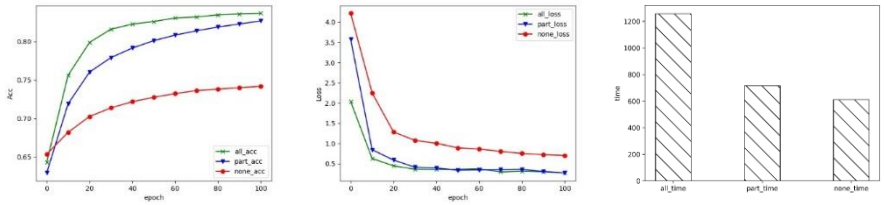

(a) Accuracy (b)Loss (c)Running time

Fig. 3. Results of 2D COVID-19 dataset with different data volumes and the same distribution

The results of 2D COVID-19 dataset are shown in Fig. 3 under the conditions of different data volumes and the same distribution. the rising trend of all-distributed is fast. Although the growth of part-distributed is slow, accuracy in the latter half of the period is similar to that of all-distributed in terms of accuracy. The difference between the accuracy of non-distributed and the other two cases is about 8%. The values of all-distributed are similar to those of part-distributed, but in terms of downward trend, all-distributed have a rapid trend in terms of loss value. The difference between the loss value of non-distributed and the other two cases is 0.6.

When the amount of data is the same and the data distribution is 2 classes (i.e. 80% are two randomly selected numbers and the remaining 20% are other numbers): the result diagram of MNIST dataset is shown in Fig. 4. The accuracy difference between all-distributed and part-distributed is 1% in terms of accuracy. The difference between the non-distributed and the other two cases is about 6%. The values of all-distributed and part-distributed are similar in the field of loss value.

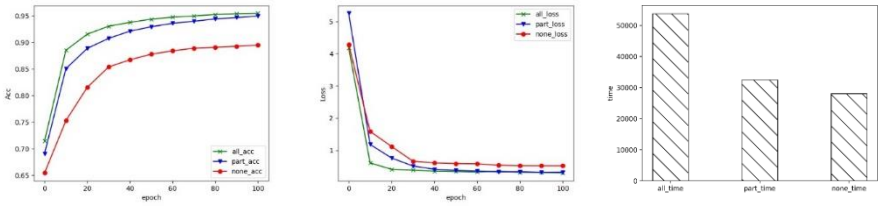

(a) Accuracy (b) Loss (c) Running time

Fig. 4. Results of MNIST dataset when the distribution is 2 classes and the number is the same

When the data volume is the same and the data distribution is 1 class (i.e. 80% is a randomly selected number and the remaining 20% is other numbers): the result diagram of MNIST dataset is shown in Fig. 5. It can be seen that the accuracy values of some-distributed and all-distributed are similar, and the difference between non-distributed and the other two cases is 7% in the accuracy. All-distributed are similar to part-distributed, and the difference between non-distributed and the other two cases is 0.5 in terms of loss value. Combined with Fig. 4, under two different distribution pattern, accuracy of some distributed is similar to that of all-distributed, which proves that this distribution strategy has strong adaptability in different distribution pattern.

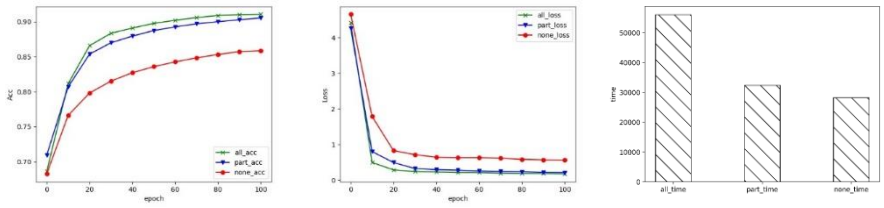

(a) Accuracy (b) Loss
(c) Running time

Fig. 5. Results of MNIST dataset when the distribution is 1 class and the number is the same

5.2 D-Unet

A. Datasets

In this section, experiments are carried out on two datasets. They are the 3D COVID-19 dataset [19] and the Liver Tumor Segmentation Challenge (LiTS)[20].

B. Evaluation Metrics

For quantitative analysis of the experimental results, several performance metrics are considered, including model parameter size, mIoU and ROC. The overall mIoU is calculated using Eq. (5).

$$mIoU = \frac{1}{k}\sum_{i=0}^{k}\frac{P_{ii}}{\sum_{j=0}^{k}P_{ij} + \sum_{j=0}^{k}P_{ji} - P_{ii}} \times 100\% \quad (5)$$

The area under curve (AUC) and the receiver operating characteristics (ROC) curve are common evaluation measures for medical image segmentation tasks. The ordinate of this curve is sensitivity and the abscissa is 1-specificity. Different points are connected into a line to form an ROC curve.

C. Experimental analysis

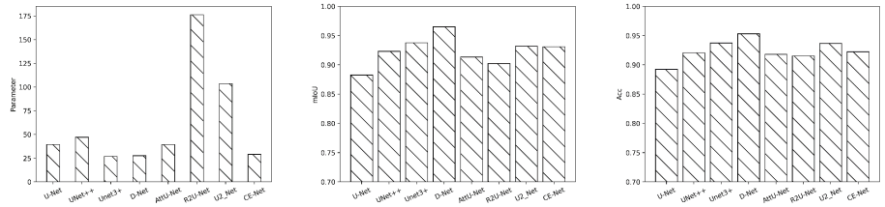

(a) Model parameter size (b) mIoU (c) Accuracy

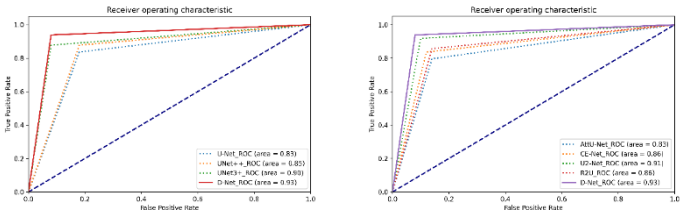

(d) ROC

Fig. 6. The renderings of different models in terms of ROC, mIoU and accuracy in the LiTS dataset

The difference in the number of model parameters is presented by histogram in Fig. 6 (a). As can be seen from the figure, the model parameters in this system are relatively small. U-Net adopts Vgg-16 skeleton, which is 39.39M; The model parameter size of UNet++ is 47.17M; The model parameter size of UNet 3+ is 26.97M; D-Net is the model parameter size of 27.63M; The model parameter size of Attention U-Net is 39.45M; The model parameter size of R2U-Net is 103.7M; The model parameter size of U^2-Net is 176.3M; The model parameter size of CE-Net is 29M. D-Net is 0.66M more than UNet 3+ model, and the parameter size does not change much. In Fig. 6 (b), it is the mIoU of each model, in which the mIoU of D-Net is 0.9653, which is 3% higher than UNet 3+. And it performs better than other models. In Fig. 6 (b), the figure shows the prediction accuracy. The prediction accuracy of D-Net is 0.9532, which is about 2% higher than UNet 3+. Comparing (b) with (c), it can be seen that the size of mIoU is positively correlated with the accuracy, which proves that this model can improve the segmentation accuracy in LiTS dataset. In Fig. 6 (d), it is the ROC curve of each model, and the area in the curve is displayed in the lower right corner. The ROC curve of D-Net wraps the ROC curve of other models, which proves that this model has good performance in disease classification.

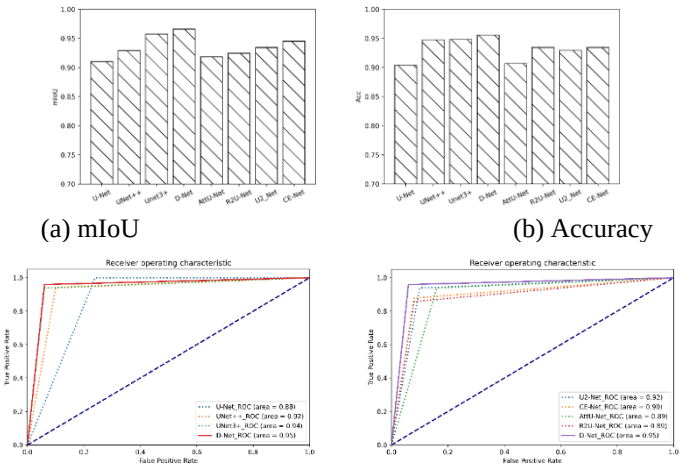

(a) mIoU (b) Accuracy

(c) ROC

Fig. 7. In the 3D COVID-19 dataset, the renderings of different models in terms of ROC, mIoU and accuracy

In Fig. 7 (a), the mIoU of D-Unet is 0.9859, which is 3% higher than UNet 3+. And it performs better than other models. In Fig. 7 (b), the accuracy of D-Net is 0.9557, about 1% higher than that of UNet 3+, which proves that this model can improve the segmentation accuracy in the COVID-19 dataset. In Fig. 7 (c), the ROC curve of D-Net wraps the ROC curve of other models, which proves that this model has a good performance in disease classification on the dataset of COVID-19.

In general, the segmentation model can still achieve high accuracy under the condition of low parameters, and realize the accurate segmentation of the image.

6 CONCLUSION

We propose a disease diagnosis framework based on federated learning to improve the accuracy of disease prediction. The framework includes data sharing strategy and image segmentation model. This framework has the following contributions: the data sharing strategy is used to overcome the phenomenon of non-IID data under the federal learning framework by issuing shared data according to certain rules; The image segmentation model not only alleviates the unknown network depth, but also provides a flexible fusion scheme. The experimental results show that the proposed disease diagnosis framework based on federated learning can effectively improve the accuracy of disease prediction.

Acknowledgment

This paper is supported by the Science and Technology Program of Inner Mongolia Autonomous Region (Grant No. 2019GG116).

References

1. Duchi J C, Hazan E, Singer Y. Adaptive subgradient methods adaptive subgradient methods for online learning and stochastic optimization[J]. Journal of Machine Learning Research, 2011, 12:2121-2159.

2. Deven M G. Building public trust in uses of Health Insurance Portability and Accountability Act de-identified data[J]. Journal of the American Medical Informatics Association Jamia, 2013(1):29-34.
3. McMahan B, Moore E, Ramage D, et al. Communication-efficient learning of deep networks from decentralized data[C]//Artificial intelligence and statistics. PMLR, 2017: 1273-1282.
4. Smith V, Chiang C K, Sanjabi M, et al. Federated multi-task learning[J]. Advances in neural information processing systems, 2017, 30.
5. Rakhlin A, Shamir O, Sridharan K. Making gradient descent optimal for strongly convex stochastic optimization[J]. arXiv preprint arXiv:1109.5647, 2011.
6. Zhao Y, Li M, Lai L, et al. Federated learning with non-iid data[J]. arXiv preprint arXiv:1806.00582, 2018.
7. Yoshida N, Nishio T, Morikura M, et al. Hybrid-FL for wireless networks: Cooperative learning mechanism using non-IID data[C]//ICC 2020-2020 IEEE International Conference on Communications (ICC). IEEE, 2020: 1-7.
8. Tuor T, Wang S, Ko B J, et al. Overcoming noisy and irrelevant data in federated learning[C]//2020 25th International Conference on Pattern Recognition (ICPR). IEEE, 2021: 5020-5027.
9. Ronneberger O, Fischer P, Brox T. U-net: Convolutional networks for biomedical image segmentation[C]//International Conference on Medical image computing and computer-assisted intervention. Springer, Cham, 2015: 234-241.
10. Oktay O, Schlemper J, Folgoc L L, et al. Attention u-net: Learning where to look for the pancreas[J]. arXiv preprint arXiv:1804.03999, 2018.
11. Alom M Z, Hasan M, Yakopcic C, et al. Recurrent residual convolutional neural network based on u-net (r2u-net) for medical image segmentation[J]. arXiv preprint arXiv:1802.06955, 2018.
12. Gu Z, Cheng J, Fu H, et al. Ce-net: Context encoder network for 2d medical image segmentation[J]. IEEE transactions on medical imaging, 2019, 38(10): 2281-2292.
13. Zhou Z, Siddiquee M M R, Tajbakhsh N, et al. Unet++: Redesigning skip connections to exploit multiscale features in image segmentation[J]. IEEE transactions on medical imaging, 2019, 39(6): 1856-1867.
14. Huang H, Lin L, Tong R, et al. Unet 3+: A full-scale connected unet for medical image segmentation[C]//ICASSP 2020-2020 IEEE International Conference on Acoustics, Speech and Signal Processing (ICASSP). IEEE, 2020: 1055-1059.
15. Qin X, Zhang Z, Huang C, et al. U2-Net: Going deeper with nested U-structure for salient object detection[J]. Pattern Recognition, 2020, 106: 107404.
16. Phong L T, Aono Y, Hayashi T, et al. Privacy-preserving deep learning: Revisited and enhanced[C]//International Conference on Applications and Techniques in Information Security. Springer, Singapore, 2017: 100-110.
17. Zhao J, Zhang Y, He X, et al. Covid-ct-dataset: a ct scan dataset about COVID-19 [J]. arXiv preprint arXiv:2003.13865, 2020, 490.
18. Hard A, Rao K, Mathews R, et al. Federated learning for mobile keyboard prediction[J]. arXiv preprint arXiv:1811.03604, 2018.
19. Kumar R, Khan A A, Kumar J, et al. Blockchain-federated-learning and deep learning models for COVID-19 detection using ct imaging[J]. IEEE Sensors Journal, 2021, 21(14): 16301-16314.
20. Bilic P, Christ P F, Vorontsov E, et al. The liver tumor segmentation benchmark (lits)[J]. arXiv preprint arXiv:1901.04056, 2019.